AIMS Materials Science, 11(1): 1–27.
DOI: 10.3934/matersci.2024001
Received: 04 September 2023
Revised: 21 November 2023
Accepted: 29 November 2023
Published: 22 December 2023

http://www.aimspress.com/journal/Materials

Research article

Magnetic characteristics of sengon wood-impregnated magnetite nanoparticles synthesized by the co-precipitation method

Saviska Luqyana Fadia[1], Istie Rahayu[1,*], Deded Sarip Nawawi[1], Rohmat Ismail[2], Esti Prihatini[1], Gilang Dwi Laksono[1] and Irma Wahyuningtyas[1]

[1] Department of Forest Products, Faculty of Forestry and Environment, IPB University, Bogor 16680, Indonesia
[2] Department of Chemistry, Faculty of Mathematics and Natural Science, IPB University, Bogor 16680, Indonesia

* **Correspondence:** Email: istiesr@apps.ipb.ac.id.

Abstract: This study was conducted to synthesize magnetic wood through the ex situ impregnation method of magnetite nanoparticles and analyze its physical properties and characterization. The process was initiated with the synthesis of magnetite nanoparticles by the co-precipitation method and the nano-magnetite was successfully synthesized with a particle distribution of 17–233 nm at an average size of 75 nm. Furthermore, the impregnation solution consisted of three different levels of magnetite nanoparticles dispersed in furfuryl alcohol, untreated and furfurylated wood for comparison. Sengon wood (*Falcataria moluccana* Miq.) was also used due to its low physical properties. The impregnation process was conducted by immersing the samples in the solution at a vacuum of –0.5 bar for 30 min, followed by a pressure of 1 bar for 2 h. There was also an improvement in the physical properties, such as weight percent gain, bulking effect, anti-swelling efficiency and density, while the water uptake continued to decrease. Additionally, magnetite nanoparticles appeared in wood microstructure image, supported by the result of ferrum content in chemical element analysis. The results showed that chemical change analysis proved the presence of Fe–O functional group cross-linked with wood polymer. The diffractogram also reported the appearance of magnetite nanoparticles peak and a decrease in crystallinity due to an increase in the concentration. Based on the analysis, sengon wood was classified as a superparamagnetic material with soft magnetic characteristics and the optimum treatment was furfurylated-magnetite 12.5% wood.

Keywords: furfuryl alcohol; magnetic wood; magnetite nanoparticles; physical properties; sengon wood; wood modification

1. Introduction

The expansion of wireless-based technology is unfavorable to the environment and human health because of its electromagnetic wave pollution [1]. Electromagnetic waves are known to be sourced from radio waves, radar waves, microwaves, UV light, X-rays and gamma rays [2]. According to Smawardika [3], this wave can cause physiological problems in the human body. To reduce the risk of exposure, it is necessary to possess a material capable of absorbing the pollution emitted by electronic instruments. Several parameters, such as weight, thickness and density, are important to affect the electromagnetic wave absorption by the materials, especially single-phase magnetic materials. Single-phase magnetic materials are materials that exhibit magnetic properties in one phase. The weight and thickness of the material are known to determine the amount of electromagnetic energy absorbed by the material, while the density of the material affects the frequency range of electromagnetic waves absorbed by the material. So, high-density and lightweight materials are preferred for shielding material applications. However, there are limitations on the performance of materials with these characteristics, for example, high-density materials have a narrow absorption bandwidth, while lightweight materials have low absorption efficiency [4]. Gao et al. [5] also reported that the increasing material thickness will lower the effective absorbing frequency and improve the reflection loss value, so this condition can make the devices quickly degrade because of the excessive temperature rise.

One example of a single-phase magnetic material is iron (Ferrum) [6]. Iron is a ferromagnetic material commonly used in electromagnetic wave absorption applications due to its high magnetic permeability and low electrical conductivity [7]. The form of iron oxide compounds used for electromagnetic wave absorbers is magnetite (Fe_3O_4). Magnetite is a magnetic material that has excellent electromagnetic wave absorption properties. The mechanism of magnetite absorbing electromagnetic waves is due to the loss of magnetic properties of the material [8]. Magnetite nanoparticles, with a particle size of less than 100 nm, have better electromagnetic wave absorption properties than bulk magnetite. The high surface area of magnetite nanoparticles can absorb electromagnetic energy more efficiently and the small particle size can increase the absorption level over a wider bandwith range [9]. The magnetic moment of a magnetic material is affected by the magnetic field it produces when an electromagnetic wave passes through it. This phenomenon is known as oscillation. The oscillation converts electromagnetic energy into heat, which is then dissipated by the material [10]. Hence, to overcome this problem, it is needed to fabricate multiphase magnetic materials by installing other conductive materials. Therefore, the dielectric constant value becomes lower and its permittivity is relatively high, ensuring better impedance [11,12]. With these benefits, biomaterial from carbon with various structures and phases is a suitable candidate with several properties of magnetic materials, such as lightweight, low density, abundant resources, high electrical properties, as well as chemical and thermal stabilization [13–18].

The multi-functional biomaterial is developed for various purposes because of its eco-friendly characteristics, such as magnetic wood. This possesses considerable promise as a biomaterial, renowned for its capacity to absorb electromagnetic waves, show magnetic properties and serve as an

efficient heat conductor. Consequently, it can obtain applications within a diverse range of industries including electronics, the military, healthcare instrumentation and green building construction [19–23]. Previous studies also reported magnetic wood applications in electronic devices, furniture coatings and interior decorations of houses [19,22–25]. This wood can be synthesized by combining with particles in several ways, such as impregnation, mixing sawdust with magnetic powder and coating using magnetic material [26]. Furthermore, [27,28] succeeded in producing magnetic wood using magnetite nanoparticles through in-situ impregnation. Magnetite nanoparticles synthesized using weak base ammonium hydroxide (NH_4OH) were bigger than those using strong base NaOH. This was because NH_4OH generated a small number of magnetic nuclei supporting crystal growth and producing particles of similar size [29].

Sengon (*Falcataria moluccana* Miq.) is one of the focuses of studies to be developed as a biomaterial resource in the future. This is because the wood has low dimensional stability and is easily degraded by insects and fungi [30–33]. Therefore, it is often discussed because of the limited use of plywood, packaging, lightweight construction and furniture [34,35]. Previously, sengon wood was used to fabricate magnetic wood using commercial magnetite nanoparticles impregnation which resulted in high physical properties and characteristics [36]. However, magnetite nanoparticles impregnation dispersed in demineralized water cannot improve wood properties. This is occurred because water is a universal solvent used as a solvent in wood in certain conditions. For example, water-based wood fillers are generally mixtures containing cellulose, wood fiber, or gypsum. These materials can be easily dry in about 15 min, and clean-up requires only soap and water [37]. Based on this research, water is still used as a comparison solvent even though it cannot dissolve magnetite completely. Hence, organic chemicals were needed to disperse magnetite nanoparticles [38].

Furfuryl alcohol is an eco-friendly organic chemical with high polarity [39,40]. Furfuryl alcohol is used in the wood modification process to improve wood properties. it has a small molecular size, which allows it to penetrate the wood and undergo polymerization in the cell wall. This polymerization can be carried out using catalysts, heat, or radiation [41]. Furfuryl alcohol greatly maintained the wood dimension by about 85% for Japanese cedar (*Cryptomeria japonica*) and Scots pine (*Pinus sylvestris* L.) specimens and prevented the leaching of chemicals from wood [41]. The polymerization of furfuryl alcohol in wood potentially provides a certain degree of protection against various environmental factors including magnetite nanoparticles that are soluble in furfuryl alcohol and have been impregnated into wood from acids and alkalis degradation [42]. Previously, the interactions between furfuryl alcohol and magnetite nanoparticles have been reported. Magnetite nanoparticles act as a homogeneous catalyst in the hydrogenation reaction of furfural to furfuryl alcohol. This catalyst showed high catalytic furfural transfer hydrogenation activity, furfuryl alcohol selectivity, high reusability and furfuryl alcohol can dissolve magnetite perfectly [43–45]. A homogeneous catalyst is a catalyst with the same phase as the reactants and is obtained by dissolving the catalyst and reactants in the same solvent [44]. Additionally, the magnetic properties of wood materials were also reported to be increased due to furfuryl alcohol addition in magnetite nanoparticle impregnation into the wood [46]. It is because this alcohol was used as a dispersant of magnetite nanoparticles to form a colloidal phase penetrating deeper into wood. This modification treatment promoted sengon wood to become high physical properties building material [47,48]. Therefore, this study was conducted to synthesize magnetic wood by the impregnation process using furfuryl alcohol combined with magnetite nanoparticles, manufactured by the co-precipitation method.

2. Materials and methods

2.1. Materials

A six-year-old Sengon wood (*Falcataria moluccana* Miq.) was obtained with a diameter of 35 cm free branch height from a community forest in Bogor, West Java. The chemicals used in this study were $FeCl_3 \cdot 6H_2O$, $FeCl_2 \cdot 4H_2O$, ammonium hydroxide (NH_4OH), ethylenediaminetetraacetic acid (EDTA), furfuryl alcohol (Sigma Aldrich, St. Louis, MO, USA) and additional supplies included pH paper and demineralized water.

2.2. Methods

2.2.1. Wood sample preparation

The log of sengon wood was cut into 2 × 2 × 2 cm without distinguishing the portion of sapwood and heartwood [49]. A total of 50 samples was required with 10 replications for each treatment. These samples were used for the physical properties tests including weight percent gain, bulking effect, anti-swelling efficiency, water uptake and density.

2.2.2. Synthesis of nano-magnetite

According to previous studies [27,28,50], the synthesis of magnetite nanoparticles initiated by mixing $FeCl_3 \cdot 6H_2O$ and $FeCl_2 \cdot 4H_2O$ into 200 mL demineralized water based on mole ratio calculation of Fe^{2+} and Fe^{3+} = 1:1.6. 0.292 g of EDTA dissolved in 100 mL of demineralized water was added to the solution and stirred using a magnetic stirrer for 5 min. The solution was vacuumed at 1 bar for 15 min and NH_4OH was slowly added until the pH reached 12 to form a black precipitate known as magnetite nanoparticles. Subsequently, the neutralization process of synthesized magnetite nanoparticles was carried out by washing the solution with demineralized water. The washing process was conducted by putting synthesized mixture into a 50 mL centrifuge tube and centrifuging at 5000 rpm for 15 min. The liquid phase of the centrifugation results was separated and 40 mL of demineralized water was added to the centrifuge with the same speed and time conditions. In the first stage, 40 mL of a mixture of solution containing magnetite precipitates under pH 12 conditions were centrifuged and the liquid was discarded. In the second stage, 40 mL of deionized water was added to the remaining sediment from the previous stage, then centrifuged and the liquid was discarded. The second stage was carried out in three repetitions. This repetition was estimated in the laboratory, if approximately 1 mL of solid solution at pH of 12 remains in the first stage, which is then washed three times and diluted 64000 times (40 × 40 × 40 dilution factor). pH 12 contains an $OH^- = 10^{-2}$ M concentration, so only 1000 times dilution is needed to reach pH 9 with an $OH^- = 10^{-5}$ concentration (pH = 14 – pOH so pH = 14 – (–log 10^{-5}) = 14 – 5 = 9). After washing the solution until pH 9, then put the magnetite nanoparticles in an oven at 40 °C.

2.2.3. Preparation of impregnation solution

The solution consists of magnetite nanoparticles and dispersant (furfuryl alcohol: demineralized water in 1:1 mole ratio) determined in w/v (g/mL) to obtain optimal results. Furthermore, three levels of magnetite nanoparticles concentration were prepared, including 7.5%, 10% and 12.5%. The solution was mixed by a sonicator (CGOLDENWALL manufactured in Zhejiang, China) with an amplitude of 40% for 10 min. Although the characteristics of magnetite are insoluble in water, because the synthesized magnetite used in this study is nanometer-sized, its solubility increases due to its large surface area [51]. In addition, sonication treatment can also increase te solubility of magnetite in water [52]. For comparison, untreated and furfurylated wood were also tested in this study.

2.2.4. Fabrication of magnetic wood

The fabrication of magnetic wood was carried out by the impregnation process adopted from the previous study [21,27,28,53]. Sengon wood samples were oven-dried at 103 ± 2 ℃ until the constant weight was achieved. This process started with immersing the samples in the solution containing synthesized magnetite nanoparticles and FA at a vacuum of –0.5 bar for 30 min followed by a pressure of 1 bar for 2 h. After impregnation, the samples were wrapped with aluminum foil and kept at room temperature for 12 h. The foil was removed from wood and placed in an oven at 65 ℃ for 12 h before drying at 103 ± 2 ℃ to obtain a constant weight.

2.3. The physical properties of magnetic sengon wood

The physical properties tested on sengon wood were weight percent gain, bulking effect, anti-swelling efficiency, water uptake and density [54–56]. The weight percent gain formula was defined by Eq 1 below:

$$WPG(\%) = \frac{W_1 - W_0}{W_0} \times 100 \quad (1)$$

where W_0 is the oven-dried weight of samples before the impregnation (g), and W_1 is the oven-dried weight of samples after the impregnation (g). Then, bulking effect of sengon wood after impregnation process was determined using Eq 2:

$$BE(\%) = \frac{V_1 - V_0}{V_0} \times 100 \quad (2)$$

where V_0 is the oven-dried volume of samples before the impregnation (cm^3) and V_1 is the oven-dried volume of samples after the impregnation (cm^3). Anti-swelling efficiency was carried out by soaking the specimens in water continuously, and was calculated by following formula (Eq 3):

$$ASE(\%) = \frac{S_u - S_t}{S_t} \times 100 \quad (3)$$

where S_u is the volume shrinkage of the untreated sample and S_t is the volume shrinkage of the treated samples. Water uptake value was determined using Eq 4:

$$WU(\%) = \frac{W_2 - W_0}{W_1} \times 100 \quad (4)$$

where W_1 is the oven-dried weight samples after impregnation (g) and W_2 is the weight of sample after being immersed for 24 h (g). Density was calculated before and after treatment and then determined using Eq 5:

$$\rho(kg/m^3) = \frac{Sample\ weight}{Sample\ volume} \tag{5}$$

where W_1 is the oven-dried weight samples after impregnation (g) and V_1 is the oven-dried volume samples after impregnation (cm^3).

2.4. Characterization of magnetic sengon wood

2.4.1. Particle size analyzer (PSA)

A total of 10 mg of synthesized magnetite nanoparticles dissolved in 100 mL of demineralized water. Furthermore, the solution was stirred for 15 min using a sonicator, according to Gerasimov et al. [57]. A 100 ppm concentration of magnetite nanoparticles was analyzed for particle size using PSA (Beckman Coulter LS 13 320 XR).

2.4.2. Scanning electron microscopy (SEM)-energy dispersive X-ray spectroscopy (EDX)

The morphology of sengon wood was examined under SEM (ZEISS EVO10 series). In this context, wood sample was cut into 0.5 × 0.5 × 0.5 cm in the tangential plane, placed on the conductor adhesive, sputtered with the gold as an electrically conductive metal and observed at 20 kV. To determine the chemical component of the treated wood, the EDX analysis was also carried out using ZEISS SmartEDX.

2.4.3. Fourier transform infrared spectrometry (FTIR)

Changes in the functional group of sengon wood due to impregnation were qualitatively evaluated by FTIR (Perkin-Elmer Spectrum One). The sawdust was ground to a size of 100 mesh and embedded in potassium bromide pellets (KBr). Meanwhile, this pellet was scanned in the wavenumber of 4000−400 cm^{-1} in a resolution of 4 cm^{-1} for 32 scans.

2.4.4. X-ray diffraction (XRD)

This study used XRD PANalytical AERIS to measure the degree of crystallinity and crystal size. Wood sample was sliced about 1 mm thick in the tangential plane. The parameters used were Cu anode, 40 kV voltage, 30 mA current and 2θ scan range 5−80° for crystallinity and 5−90° for phase analysis with the scanning speed at 2°/step. Additionally, XRD patterns of Fe_3O_4 nanoparticles were analyzed according to JCPDS No. 04-0755.

2.4.5. Vibrating sample magnetometry (VSM)

Magnetic properties of sengon wood were evaluated using VSM250 (VSM Dexing Type 250). The parameters measured include magnetization saturation (Ms), retentivity (Mr) and coercivity (Hc). The hysteresis loop was analyzed at 298–773 K in an external magnetic field of 100 Oe until 21 kOe and the sample dimension was 3.5 × 3.5 × 1 mm in the longitudinal section.

2.5. Data analysis

A completely randomized design was used to evaluate data through ANOVA. This was followed by Duncan's tests at $\alpha = 5\%$ and statistical analysis was performed by IBM SPSS 25.0.

3. Results and discussion

The synthesis of magnetite nanoparticles used the co-precipitation method with a weak base precursor of NH_4OH and EDTA as a capping agent. These chemicals can control the particle size to be smaller and have a uniform morphology [58]. The co-precipitation method was selected for the laboratory scale due to its high yield reaching 91.17% [59] and its correlation with the manufacture of magnetic wood by ex situ [28]. The addition of EDTA solution reduced surface energy and the possibility of magnetite nanoparticle agglomeration to improve the dispersibility. The molecules can change the mechanism of nucleation and growth of nanostructures, reducing nanoparticle size and supporting the stabilization which are less susceptible to oxidation [60,61]. Moreover, EDTA coating improves the adsorption capacity by increasing the surface area efficiently [62]. The sonication process was conducted to enhance the solubility of magnetite nanoparticles [63]. According to Sompech et al. [52], sonication can reduce the particle size and heat energy to increase the particle movement.

The choice of weak base NH_4OH as the precursor base used in the co-precipitation synthesis of magnetite nanoparticles was based on Peternele et al. [50]. The co-precipitation method is commonly used to synthesize magnetite from precursor materials in the form of a mixture of iron salts and bases. In this method, solutions containing precursor materials are mixed together and the pH of the solution is adjusted to induce magnetite precipitation [64]. Magnetite nanoparticles were obtained by the co-precipitation of iron (II) and iron (III) salts in aqueous media at different Fe^{3+}/Fe^{2+} ratios, with NH_4OH base solution at room temperature, this reaction shown in Eqs 6 and 7.

$$Fe^{3+} + 3OH^- = Fe(OH)_3 = FeOOH + H_2O \quad (6)$$

$$Fe^{2+} + 2OH^- = Fe(OH)_2 \quad (7)$$

The reaction between the iron salt solution and the precipitating agent in the form of a base is slightly exothermic. The Eqs 8 and 9 are the total reaction for the magnetite formation [65].

$$2FeOOH + Fe(OH)_2 = Fe_3O_4 + 2H_2O \quad (8)$$

$$2Fe^{3+} + Fe^{2+} + 8OH^- = 2Fe(OH)_3Fe(OH)_2 \rightarrow Fe_3O_4 + 4H_2O \quad (9)$$

Based on the reactions above, NH_4OH is a precursor for magnetite formation by donating hydroxy ions (OH^-). According to the transmission electron microscopy (TEM) and the Scherrer equation, the material obtained from the NH_4OH precipitating agent is more uniform than NaOH. TEM results

showed that small magnetite particles were likely embedded into larger particles when treated with NaOH. The particles formed were more uniform and monodisperse when treated with NH_4OH. Therefore, a weak base of NH_4OH should be preferentially used as a precursor base in the synthesis of magnetite nanoparticles.

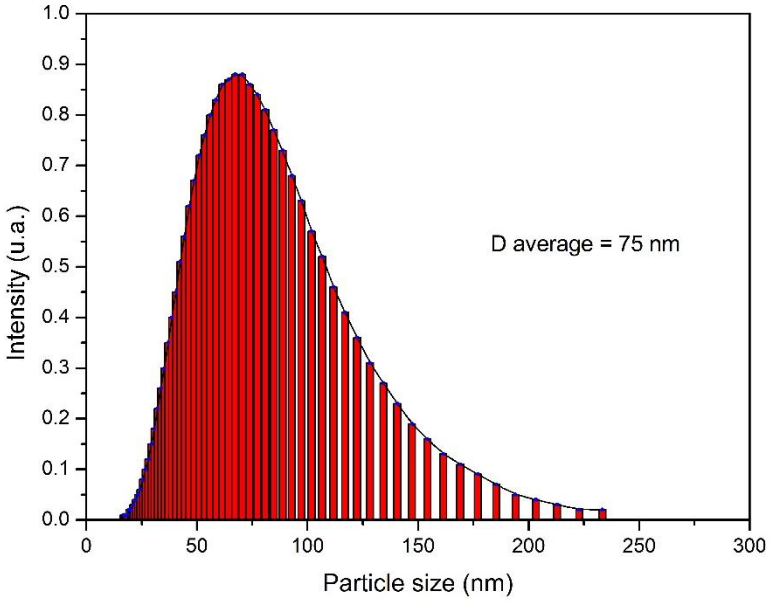

Figure 1. Size distribution of magnetite nanoparticles synthesized through the co-precipitation method with the weak base precursor of NH_4OH.

Based on Figure 1, the particle size distribution ranged from 17–233 nm with the highest intensity at 70 nm and the average was 75 nm. This showed that synthesized magnetite was classified as nanoparticle material because the size was less than 100 nm [66] and possessed the good quality to be impregnated into sengon wood by the ex situ method. The impregnation process was initiated with vacuum condition, which was defined as the condition of the tube having a very low air pressure of –0.5 bar. This condition enhanced the impregnation depth by removing air from the porous media or wood cavities [67,68], hence particles in the impregnation tube did not affect the penetration of magnetite nanoparticles and furfuryl alcohol [38,39]. The amount of magnetite nanoparticles entering wood cavities depends on the sengon wood structural anatomy. Martawijata et al. [69] stated that sengon wood has a pore diameter of 140–200 µm with oval to round in shape. There are 2–4 pores that are radially interconnected and are mostly seen solitary, with a frequency of 1–3 pores/mm^2. Based on this result, it can be suspected that magnetite nanoparticles that have a size under 140 µm successfully entered the wood cell wall. In addition, oven-drying and vacuum processes resulting in wood tends to react with chemicals entering the wood. Sengon wood is also known to have cell wall thickness and fiber length respectively of 1.55–2.19 and 1170 µm [31,70], indicating there are many empty room inside the wood. This statement is also supported by sengon wood density previously obtained was only 320 kg/m^3, affected by the cell wall thickness of wood fiber [71]. After the impregnation process was carried out, the physical properties of wood were measured by calculating weight and volume before and after treatment in percent [19].

The impregnation of three levels of magnetite nanoparticles with furfuryl alcohol as a dispersant showed significant effects in the weight percent gain, bulking effect, anti-swelling efficiency, water uptake and density of sengon wood. The enhancement of the physical properties of sengon wood is shown in Table 1. The low weight percent gain, bulking effect and density of the untreated wood were caused by no chemicals deposited in the wood cell wall after impregnation. The wood sample was originally in the condition of an oven-drying process to degrade the hydrogen bonds between cellulose and water molecules which led wood to have a moisture content of under 10% [72]. Impregnation treatment was also initiated with a vacuum process to remove air and water vapor from the wood with a certain pressure. The wood becomes more reactive to chemicals and easily to bond with. Incorporating solid inorganic materials, namely magnetite nanoparticles, is supposed to make the wood matrix firmer and dimensionally stable. However, impregnating wood using only magnetite nanoparticles and deionized water cannot affect the dimensional stability of sengon wood. Water cannot disperse magnetite nanoparticles well since the surface energy of magnetite nanoparticles remains higher so they tend to agglomerate and are difficult to disperse uniformly into the wood [73].

There was also a slight increase in the physical properties of furfurylated wood, but was insignificantly different from the untreated wood. This is because furfuryl alcohol only has a molecular weight of 98.1 g/mol, thus, furfuryl alcohol was suspected to bulk on wood surfaces and only added a slight weight and volume to sengon wood. On the other hand, magnetite nanoparticles have a molecular weight of 231.533 g/mol which can improve the weight percent gain, bulking effect and density of the wood after being combined with furfuryl alcohol. This solution forms a colloidal phase in order that interaction at the molecular level can be reached to produce wood with high dimensional stabilization from changing moisture and temperatures, indicated by the increasing anti-swelling efficiency of the furfurylated-magnetite wood. The colloid dispersed into the wood matrix will produce a large number of interfacial regions relative to the micro-composite [74]. So, the wood will have a constant dimension and is also protected from exposure to direct sunlight and biological attacks (mold, fungi, bacteria and insects) [75].

Table 1. The physical properties of sengon wood in several concentrations.

Samples	WPG (%)	BE (%)	ASE (%)	WU (%)	Density (kg/m^3)
Untreated	0.00 ± 0.02^{a}	0.99 ± 0.66^{a}	0.00 ± 0.84^{a}	72.03 ± 8.69^{c}	230 ± 10^{a}
Furfurylated wood	9.22 ± 2.66^{b}	2.82 ± 1.75^{b}	13.99 ± 371^{a}	15.01 ± 2.70^{b}	350 ± 26^{b}
FM 7.5%	144 ± 7.26^{c}	5.77 ± 1.41^{c}	69.91 ± 6.72^{b}	9.62 ± 4.16^{b}	722 ± 80^{c}
FM 10%	140 ± 7.55^{c}	4.60 ± 0.35^{c}	74.21 ± 8.22^{b}	7.14 ± 6.79^{a}	730 ± 76^{c}
FM 12.5%	150 ± 8.35^{c}	7.40 ± 0.53^{d}	74.33 ± 4.85^{b}	6.58 ± 3.01^{a}	734 ± 62^{c}

$^{a–d}$Note: Alphabetical value means significantly different based on (P-value < 0.05) Duncan's test; FM: furfurylated-magnetite wood; WPG: weight percent gain; BE: bulking effect; ASE: anti-swelling efficiency; WU: water uptake.

This caused a deep penetration and cross-linked with wood cell components to increase the volume and density [42,76]. Prihatini et al. [38] found that the impregnation using water dispersant had no different effect on the physical properties of wood. In contrast, furfuryl alcohol addition supported the process and increased the physical properties of wood. The physical properties were higher than in an earlier study [46], even though the results used the ex situ impregnation method. The enhanced anti-swelling efficiency and reduced water uptake of magnetic sengon wood were attributed

to the presence of an EDTA coating on the surface of magnetite nanoparticles. This coating effectively prevented the dissolution of nanoparticles when exposed to water. Therefore, the observed values were influenced by the increasing concentration of magnetite nanoparticles [77].

The solution containing furfuryl alcohol and magnetite nanoparticles also formed a blackish-brown resin precipitate into wood cell wall covering the pores. This formed resin also caused a darker discoloration of wood (Figure 2), as explained by previous studies [78–80]. Segmehl et al. [81] also showed the change of magnetic wood color to a strong grey metallic caused by in situ synthesis. This darkening and metallization process proved a distribution of magnetite nanoparticles in the cell wall of sengon wood.

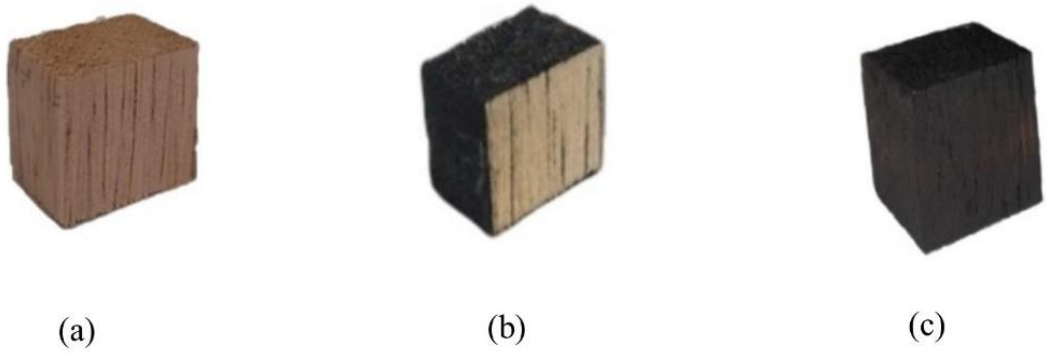

Figure 2. The visual appearance of sengon wood of (a) untreated wood, (b) furfurylated wood and (c) furfurylated-magnetite wood.

The improvement in the anti-swelling efficiency of furfurylated-magnetite wood after impregnation treatment also occurred. This was because furfuryl alcohol and magnetite nanoparticles replaced the free and bound water in the cell wall [56,82]. The sample also showed an increasing trend in anti-swelling efficiency, linear with the addition of nanoparticles concentration. Similarly, there was a slight decrease in the anti-swelling efficiency of furfurylated-magnetite 10% wood due to the partial decomposition of the cell components. In comparison with furfurylated-magnetite wood, furfurylated wood has a lower anti-swelling efficiency causing the possibility of a leaching rate during water immersion [83,84]. Therefore, the untreated and furfurylated wood could absorb water, represented by increasing the uptake. The solution penetration in wood cell wall after treatment was confirmed by SEM image in 550× magnification, as shown in Figure 3.

The results showed that the solutions containing furfuryl alcohol and magnetite nanoparticles filled the cell cavities, dispersed into the wood pores and acts as a bulking agent that having ability to bond each other and lignin as the wood chemical compounds. Wood polymers are likely a limited medium for furfuryl alcohol polymerization, leading to chain elongation and the formation of furfuryl alcohol resin within the cell wall [85]. Figure 3a shows the appearance of magnetite bulk synthesized by the co-precipitation method under SEM imaging. Nanoparticles tend to have a larger size than others due to agglomeration. Wood cavities of the untreated wood sample (Figure 3b) were visibly not covered by chemicals due to their reduced physical properties among the others. In furfurylated wood (Figure 3c), the cavities were covered by furfuryl alcohol polymer. These samples were not provided for the existence of magnetite nanoparticles and furfurylated-magnetite wood (Figures 3d–f)

showed penetration in the cell wall represented with a green color. The variations of concentration also affected the amount of element Fe which was increased with the addition of magnetite nanoparticles in furfurylated-magnetite wood, as shown in Figure 4. EDX analysis was carried out to determine the accumulation deposited in wood pores according to the SEM imaging results. In addition, accurate data was produced on the determination of elements in tissues, cells, or other samples in correlation with SEM imaging [86]. Elemental analysis with inductively coupled plasma mass spectrometry (ICP-MS) was not performed due to its destructive nature [87,88]. Based on the study of Bartz et al. [88], the results obtained from SEM-EDX could be compared with the qualitative analysis with ICP-MS.

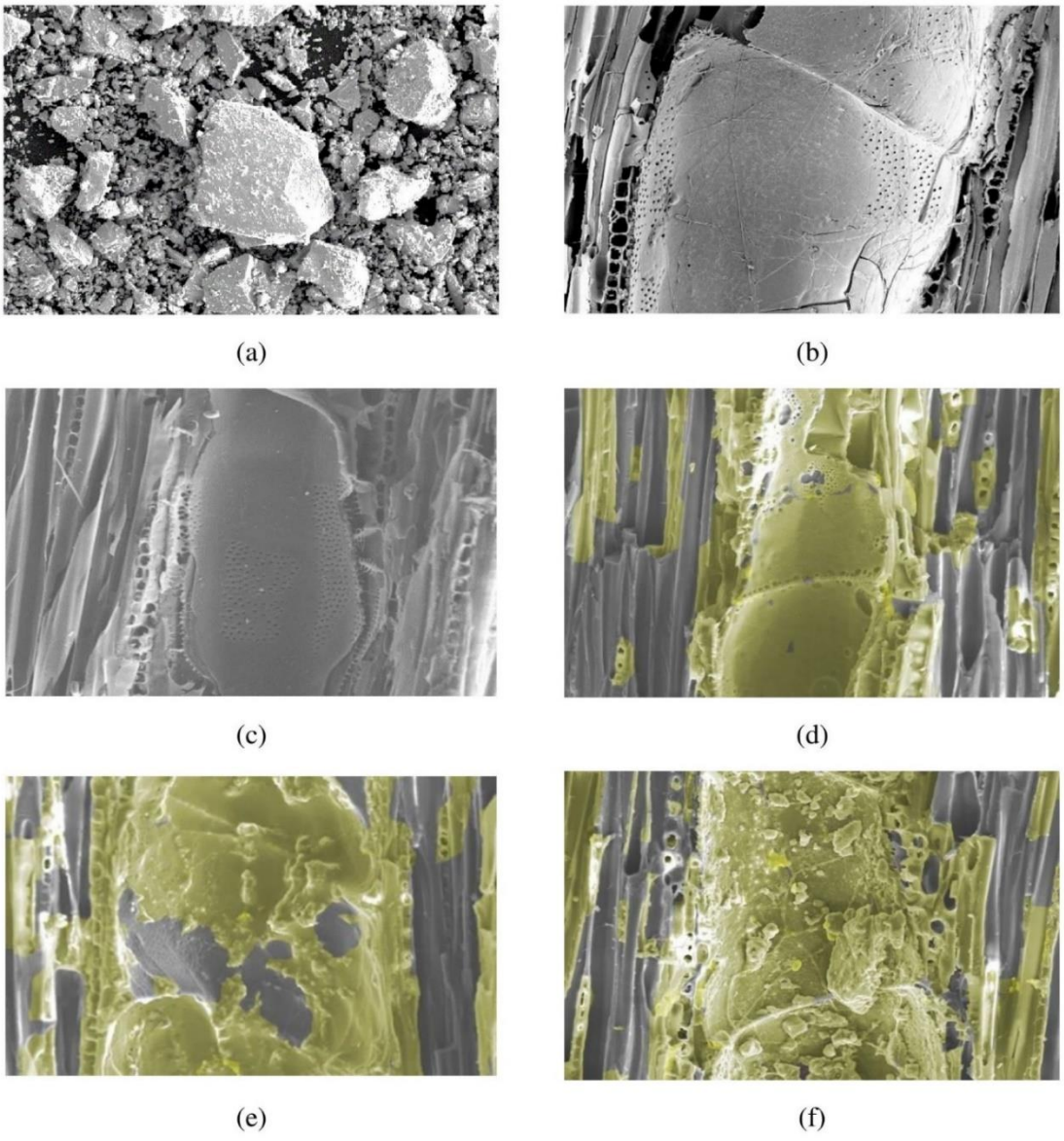

Figure 3. SEM imaging results of (a) magnetite bulk, (b) untreated wood, (c) furfurylated wood, (d) furfurylated-magnetite 7.5% wood, (e) furfurylated-magnetite 10% wood and (f) furfurylated-magnetite 12.5% wood.

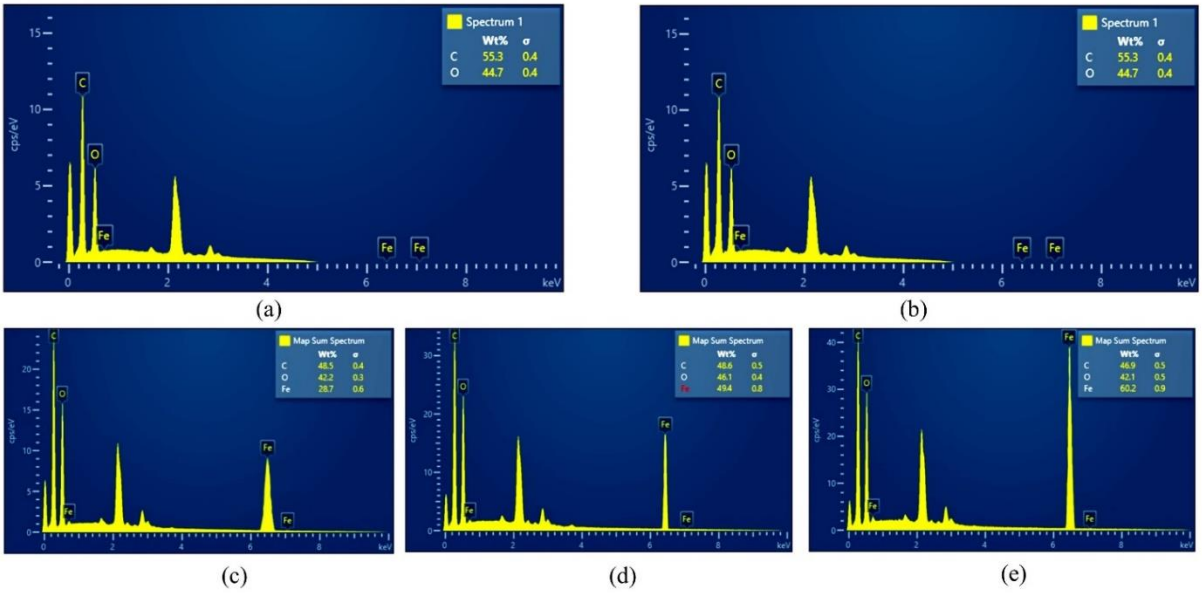

Figure 4. EDX results of (a) untreated wood, (b) furfurylated wood, (c) furfurylated-magnetite 7.5% wood, (d) furfurylated-magnetite 10% wood and (e) furfurylated-magnetite 12.5% wood.

The amount of Fe elements in magnetic sengon wood was known to be higher with the increasing concentration. Magnetite nanoparticles were synthesized using a weak base of NH_4OH resulting in a similar size. The addition of EDTA also encapsulated magnetite nanoparticles to prevent agglomeration and oxidation reactions [60]. Magnetite nanoparticles dispersed by furfuryl alcohol formed a suspension in small particles to increase the reactivity and penetration level. This condition caused the increasing weight percent gain, bulking effect and density of sengon wood after the impregnation process as shown in Figures 3d–f. Furfurylation also maintained the interaction of the solution and the lignin component of sengon wood to reduce the risk of honeycomb occurrence [89,90]. Additionally, there were morphology changes in wood cavities due to the pressure exerted on wood, forcing magnetite nanoparticles to penetrate deeper and causing the breakdown of the cell walls. The quantity of Ferrum element that was deposited in the cell wall is written in Table 2.

Table 2. The amount of Fe elements contained magnetic sengon wood in several concentrations.

Samples	Fe contain (wt.%)
Untreated	0
Furfurylated wood	0
FM 7.5%	28.75
FM 10%	49.47
FM 12.5%	60.23

FM: Furfurylated-magnetite wood.

Changes in the chemical composition of modified sengon wood using furfuryl alcohol as a dispersant were analyzed by the FTIR spectrum as shown in Figure 5. The absorption bands of the O–H

functional groups were detected at wave numbers of 3380–3387 cm^{-1}, following the results of the prior study [91,92]. The existence of the O–H groups was related to characteristics of water molecules in the liquid phase which interacted with sengon wood polymer. The intensity decreased with the addition of magnetite nanoparticles concentration, associated with the lowering water uptake in sengon wood. There was an absorption band in a wave number of 2916 cm^{-1} in the untreated samples before shifting to a wave number of 2902 cm^{-1} in furfurylated and furfurylated-magnetite wood samples. This was identified as aliphatic C–H groups of cellulose and hemicellulose according to the report of preceding studies [93–95]. In addition, a peak at wave number 1738 cm^{-1} in untreated wood was identified as the presence of C=O groups originating from the breaking of the ester bonds in hemicellulose and lignin chains [46]. Furfuryl alcohol addition also reduced the intensity of C=O groups in treated wood samples.

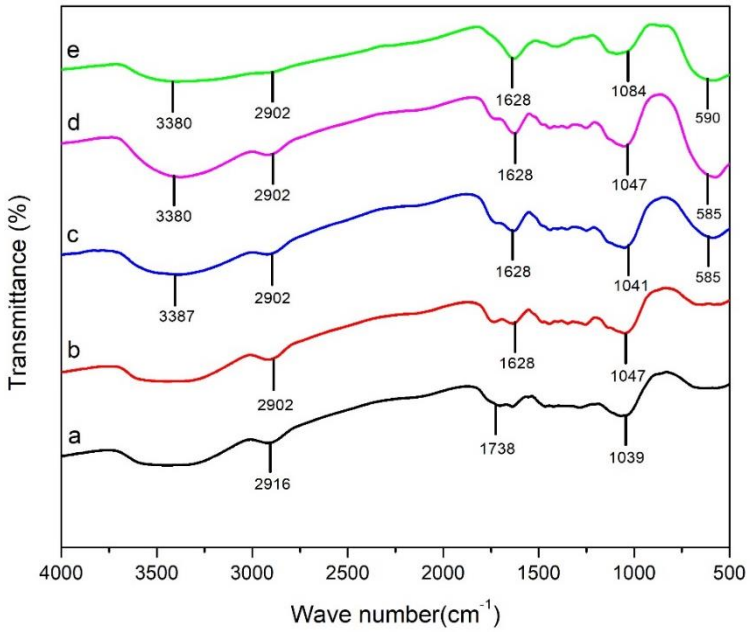

Figure 5. FTIR spectrum of sengon wood (a) untreated, (b) furfurylated wood, (c) furfurylated-magnetite 7.5%, (d) furfurylated-magnetite 10% and (e) furfurylated-magnetite 12.5%.

The increasing intensity of the C=C functional group at the wave number 1628 cm^{-1} showed the effect of furfuryl alcohol addition to the vibration of the aromatic furan ring [96]. Furthermore, the polymerized furfuryl alcohol showed 2,5-substituted furan ring vibrate [27,97]. The next peak was found at wave numbers 1039–1084 cm^{-1} confirmed as the presence of the C–O functional groups [80]. The successful dispersion of magnetite nanoparticles into the wood cavity was shown by the strong vibration of the Fe–O groups at wave numbers 585 and 590 cm^{-1}. According to a previous study [98], the strong and weak Fe–O peaks of commercial magnetite nanoparticles were detected at wave numbers 580 and 436 cm^{-1}. The impregnation treatment with furfurylation destroyed the wood cell wall by breaking the side chains in lignin as wood adhesive in the cell wall [42]. Lou et al. [99] explained that lignin content affected the absorption efficiency of magnetite nanoparticles and the Fe–O vibration synthesized by the co-precipitation method appeared at 579–635 cm^{-1} [100]. Chemical analysis using Raman spectroscopy was not performed in this study. Even though both use

wave vibration to detect the chemical composition of the materials, Raman spectroscopy can detect chemical compounds, whereas FTIR only detects the functional groups in the materials [101]. By observing the wood cell walls, using FTIR is all that is needed to identify magnetite nanoparticles presence in the wood cell walls. Prihatini et al. [38] also prove the presence of magnetite nanoparticles in the wood cell wall by attracting wood with permanent magnets and resulting in a positive reaction although it used a low concentration of magnetite nanoparticles. Thus, the presence of magnetite nanoparticles in this paper is believed to be embedded in cell walls and wood cavities.

There was a decrease in intensity at the identified peak due to the successfulness of the polymerization process and the bulking effect on sengon wood. The polymerization reaction caused the rearrangement of the crystalline structure of cellulose because of the opening of aromatic rings and the formation of hydrogen bonds. There were peaks of 2θ = 35.23 (I_{311}), 44.84 (I_{400}), 56.27 (I_{511}) and 62.33° (I_{440}) associated with the presence of magnetite nanoparticles in furfurylated-magnetite wood (Figure 6a). These peaks were confirmed to be magnetite peaks as shown in the powder data file (PDF) card in Figure 6b. These peaks were also related to an increase in the weight percent gain and bulking effect of magnetic sengon wood used as a dispersant to distribute magnetite nanoparticles [102]. Conversely, the crystal peaks at 2θ = 15.45 (I_{020}) and 22.92° (I_{012}) were identified by the results of previous study [27,103] as characteristics of cellulose in sengon wood, approaching the peak of cellulose shown in Figure 6c. For further information, the diffractograms of sengon wood with PDF card of magnetite nanoparticles and cellulose are shown below.

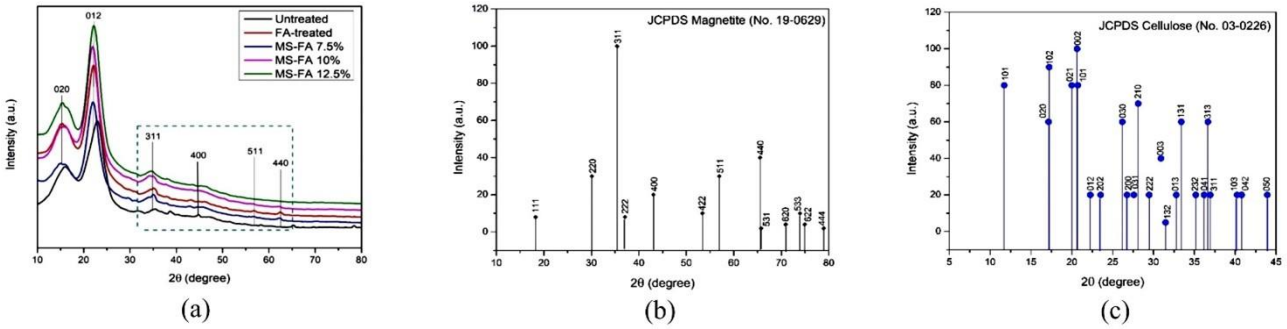

Figure 6. The diffractogram of (a) sengon wood in several concentrations, (b) PDF card of magnetite nanoparticles and (c) PDF card of cellulose.

The degree of crystallinity is the parameter affecting the physical properties and strength of wood, which was influenced by the size of the crystals' formation during synthesis. The composition of wood polymers, such as cellulose, hemicellulose and lignin, also contributed to determining the crystallinity. The amorphous area of hemicellulose and lignin caused the widening of the crystallite peak [104]. Fadli et al. [105] found the increasing temperature and stirring rate when the synthesis of magnetite nanoparticles also affected the crystallinity of magnetite nanoparticles. The higher crystalline phase tends to enhance the physical properties and strength of a material. Meanwhile, the acid treatment leads to a decrease in crystallinity to degrade wood cellulose [106,107]. The diffractogram shown in Figure 6a was used to determine the crystal size in magnetic sengon wood. According to [98], the measurement of crystalline diameter was carried out through the Scherrer equation, as written in the following formula (Eq 10):

$$D = \frac{K\lambda}{\beta \cos\theta} \tag{10}$$

The formula above is the relationship between the broadening of the diffraction peak (β), defined as the full width of the peak at half maximum (FWHM) and the crystal size (D). The wavelength of X-rays (0.15418 nm) is symbolized by λ, while K is the Scherrer constant (0.89) and θ is the Bragg diffraction angle [27]. The degree of crystallinity and crystalline diameter of magnetite nanoparticles in sengon wood is presented in Table 3.

Table 3. The degree of crystallinity and magnetite crystalline diameter of sengon wood in several concentrations.

Samples	Degree of crystallinity (%)	Crystalline size (nm)
Untreated	66.55	-
Furfurylated wood	62.21	-
FM 7.5%	50.35	24
FM 10%	44.71	24
FM 12.5%	30.39	37

FM: furfurylated-magnetite wood.

Based on Table 3, untreated and furfuryl alcohol-treated wood have higher crystallinity. This was because the measurement of the degree was carried out on cellulose. Therefore, wood without treatment was the standard value for magnetic sengon and furfurylated wood. The crystal size value is an approximation of the size of magnetite crystals deposited in wood after the impregnation process. Untreated and furfurylated wood did not contain nanoparticles, hence the crystal size was written as zero and wood crystallinity was inversely proportional to the concentration. This was caused by the addition of furfuryl alcohol, which had amorphous characteristics of reducing the size of the deposited particles. Previously, crystalline sizes larger than 50 nm would lose their magnetic properties due to the influence of gravitational forces [108]. The size of magnetite nanoparticles crystalline from this study was larger than the previous result [28] which was also synthesized by the co-precipitation method using the strong base NaOH precursor. Meanwhile, NH_4OH was known to make smaller particles of magnetite as compared to NaOH [109]. According to Fadia et al. [110], the crystal size was directly proportional to magnetite nanoparticles concentration. Magnetite nanoparticles are subjected to oxidation reactions as explained by the following chemical reaction equation (Eq 11) [111]:

$$4Fe_3O_4 + O_2 \rightarrow 6\gamma\text{-}Fe_2O_3 \rightarrow 6\alpha\text{-}Fe_2O_3 \tag{11}$$

Based on the data of magnetite diffractogram (JCPDS No. 04-0755) [112] compared to the maghemite (α-Fe_2O_3) (JCPDS No. 39-1380), the diffractogram of magnetic wood does not have a maghemite phase peak. Various efforts have been made to avoid the oxidation process, specifically in nanoparticles synthesis process. The addition of EDTA was carried out to increase the stabilization of magnetite nanoparticles and reduce the level of susceptibility to oxidation reactions. This condition occurred because the interaction with oxygen was reduced due to the functionalization of EDTA [60]. In addition, the impregnation process was conducted through vacuum technology by removing air from

the impregnation tube [113] and the oxygen concentration became lower decreasing the possibility of an oxidation reaction.

Magnetic characterization test resulted in a hysteresis loop of sengon wood at various concentrations as shown in Figure 7. The results showed that 12.5% furfurylated-magnetite had an elongated and narrow hysteresis loop compared to other samples with short and widened loops. According to Tang and Fu [114], this loop showed that magnetic sengon wood had superparamagnetic properties.

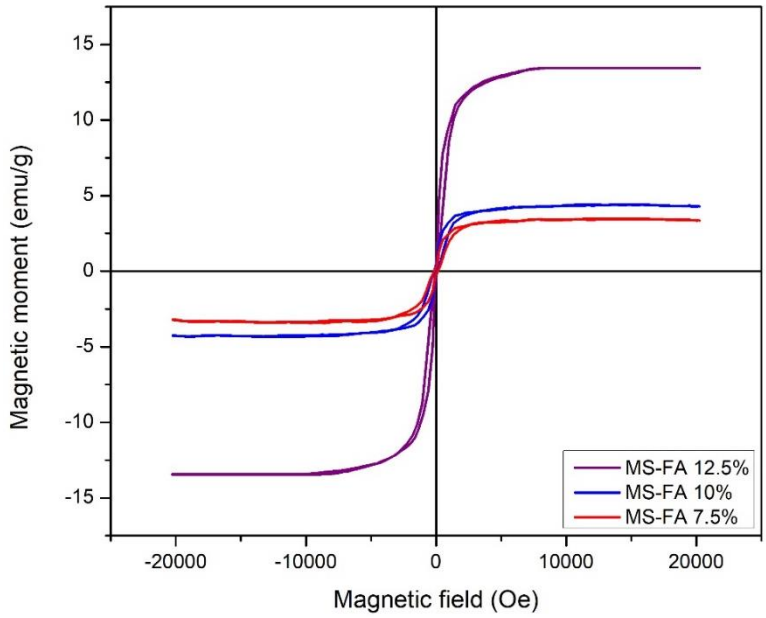

Figure 7. The hysteresis loop of magnetic sengon wood in several concentrations.

The untreated and furfurylated wood samples were not tested in this section. This was because the instrument was unable to read magnetic parameters generated. In addition, properties were affected by the changes in temperature and the portion of the non-magnetic materials [115,116]. Magnetite phase must be maintained due to its highest saturation magnetization (Ms), hematite (γ-Fe_2O_3) and the maghemite (α-Fe_2O_3) values, namely 90–100, 0.3 and 60–80 emu/g, respectively [117]. Furthermore, magnetic properties of wood was decreased through the use of magnetite. The values of the saturation magnetization, retentivity and coercivity of magnetic sengon wood have also been measured as shown in Table 4.

Table 4. The saturation magnetization, retentivity and coercivity of magnetic sengon wood.

Samples	Ms (emu/g)	Mr (emu/g)	Hc (Oe)
FM 7.5%	3.37	0.27	4.79×10^{-4}
FM 10%	4.28	0.38	2.56×10^{-4}
FM 12.5%	13.45	0.42	1.56×10^{-4}

FM: furfurylated-magnetite wood; Ms: saturation magnetization; Mr: retentivity and Hc: coercivity.

The saturation magnetization value with the addition of magnetite nanoparticles concentration and the highest saturation was obtained in furfurylated-magnetite 12.5% wood. According to previous

studies [118], the 35 nm magnetite nanoparticles were successfully synthesized with ionic solutions at room temperature and produced a saturation magnetization value of up to 25 emu/g. The values obtained in this study were lower due to the presence of wood as a non-magnetic substrate, which resulted in a decrease. Likewise, the retentivity value was in line with the increase in saturation magnetization. This value was reported to be directly proportional to the resistance of magnetic properties of the modified wood [119]. Conversely, the coercivity values presented in Table 4 possessed the same accuracy at 10^{-4} and this continued to decrease with the addition of higher concentration. Characteristics were the factors that caused magnetic sengon wood to have superparamagnetic properties [120]. The coercivity value generated from weak base precursor NH_4OH was 78 emu/g [50]. In this context, furfurylated-magnetite 12.5% wood was the easiest wood to magnetize by an external magnetic field and the most difficult to remove magnetic properties compared to others [121]. According to Inoue and Kong [118], magnetic materials are classified into soft and hard. Soft magnetic materials are characterized by coercivity values ranging from 10^{-1}–10^{-2} A/m and high permeability, while hard magnetic materials possess high retentivity and coercivity values between 103–105 A/m. Therefore, furfurylated-magnetite 12.5% wood belonged to the category of soft magnetic material.

This study also verified the correlation of magnetite nanoparticles concentration and weight percent gain with the saturation magnetization shown in Figure 8. The black line in the graph signifies that an increase in concentration has a favorable impact on saturation magnetization. Similarly, the blue line shows that an increase in weight percent gain has a positive effect. The higher concentration of magnetite nanoparticles and weight percent gain value require a small external magnetic field applied to wood [122]. Kirupakar et al. [123] explained that the higher magnetization caused the increase of induced current due to the good distribution of magnetite nanoparticles in wood interior. Saturation magnetization value was also influenced by the particles and crystallite size of the materials. Therefore, many crystals make up this material due to larger ratio, resulting in a wide magnetic domain [114].

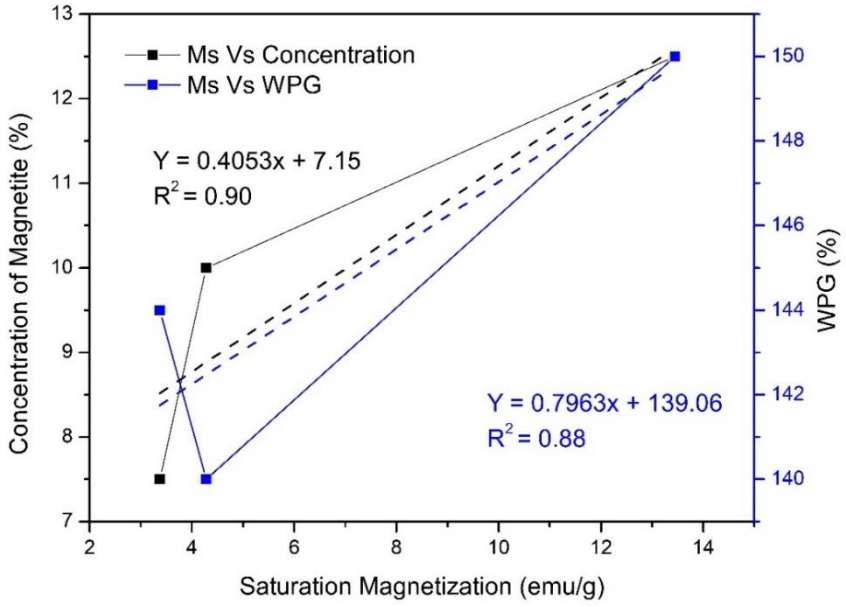

Figure 8. The correlation of the saturation magnetization with a concentration of magnetite nanoparticles and weight percent gain of magnetic sengon wood.

Several studies have mentioned the use of soft magnetic materials, which possess a high frequency of electromagnetic and lightweight features [124]. Wood with soft magnetic characteristics possessed great prospects for application as core materials in power inductors and transformers, sensors, active fillers, electromagnetic noise suppressors and other devices. This was because of the excellent initial permeability, flux density, Curie temperature and low power loss [125–127]. In addition, magnetic wood was also used for medical instruments, building and furniture materials, wastewater purification, as well as serving as an electromagnetic shielding material [128].

4. Conclusions

In conclusion, magnetite nanoparticles synthesized using a weak base of NH_4OH were reported to possess a positive effect on the physical properties of impregnated sengon wood. Furthermore, the use of furfuryl alcohol as a dispersant was more effective in increasing magnetite nanoparticles' penetration. The results of wood microstructure images proved the presence of magnetite nanoparticles in the cell wall after the impregnation process. This was supported by chemical analysis, stating the presence of metallic Fe with an increased percentage due to the addition of magnetite nanoparticles concentration. The Fe–O group was also found in the polymers, strengthening the evidence for the presence of nanoparticles binding to the cell wall components. In addition, the degree of crystallinity decreased with increasing solution concentration. This also increase affected the strength of sengon wood, resulting in superparamagnetic properties and classified as a soft magnetic material. Therefore, the best treatment for magnetic sengon wood fabrication was furfurylated-magnetite 12.5% wood.

Use of AI tools declaration

The authors declare they have not used Artificial Intelligence (AI) tools in the creation of this article.

Acknowledgments

The authors are grateful to the Directorate General of Higher Education, Research, and Technology of the Ministry of Education, Culture, Research, and Technology of the Republic of Indonesia for funding this research of the Postgraduate Research-Master Thesis Research Scheme (PPS-PTM) with the (Contract number of 18905/IT3.D10/PT.01.02/M/T/2023 and 102/E5/PG.02.00.PL/2023) on 2023.

Conflict of interest

The authors declare no conflict of interest.

References

1. Mashkour M, Ranjbar Y (2018) Superparamagnetic Fe_3O_4@ wood flour/polypropylene nanocomposites: Physical and mechanical properties. *Ind Crop Prod* 111: 47–54. https://doi.org/10.1016/j.indcrop.2017.09.068

2. Sudirman AW (2020) Effect of cellphone electromagnetic wave radiation on the development of sperm. *JIKSH* 9: 708–712. https://doi.org/10.35816/jiskh.v12i2.385
3. Swamardika IBA (2009) Pengaruh radiasi gelombang elektromagnetik terhadap kesehatan manusia (suatu kajian pustaka). *MITE* 8: 1–4. https://ojs.unud.ac.id/index.php/jte/article/view/1585
4. Wang S, Ashfaq MZ, Gong H, et al. (2021) Electromagnetic wave absorption properties of magnetic particle-doped SiCN (C) composite ceramics. *J Mater Sci Mater Electron* 32: 4529–4543. https://doi.org/10.1007/s10854-020-05195-5
5. Gao K, Zhao J, Bai Z, et al. (2019) The preparation of FeCo/ZnOcomposites and enhancement of microwave absorbing property by two-step method. *Materials* 12: 3259. https://doi.org/10.3390/ma12193259
6. Lu C, Wu M, Lin L, et al. (2019) Single-phase multiferroics: New materials, phenomena, and physics. *Natl Sci Rev* 6: 653–668. https://doi.org/10.1093/nsr/nwz091
7. Zhao Z, Gao Z, Lan D, et al. (2021) MOFs-derived hollow materials for electromagnetic wave absorption : Prospects and challenges. *J Mater Sci Mater Electron* 32: 25631–25648. https://doi.org/10.1007/s10854-021-06069-0
8. Shanenkov I, Sivkov A, Ivashutenko A, et al. (2017) Magnetite hollow microspheres with a broad absorption bandwidth of 11.9 GHz: Toward promising lightweight electromagnetic microwave absorption. *Phys Chem Chem Phys* 19: 19975–19983. https://doi.org/10.1039/c7cp03292g
9. Wang F, Liu J, Kong J, et al. (2011) Template free synthesis and electromagnetic wave absorption properties of monodispersed hollow magnetite nano-spheres. *J Mater Chem* 21: 4314–4320. https://doi.org/10.1039/c0jm02894k
10. Zhang D, Cheng J, Yang X (2014) Electromagnetic and microwave absorbing properties of magnetite nanoparticles decorated carbon nanotubes/polyaniline multiphase heterostructures. *J Mater Sci* 49: 7221–7230. https://doi.org/10.1007/s10853-014-8429-3
11. Lou Z, Li Y, Han H, et al. (2018) Synthesis of porous 3D Fe/C composites from waste wood with tunable and excellent electromagnetic wave absorption performance. *ACS Sustainable Chem Eng* 6: 15598–15607. https://doi.org/10.1021/acssuschemeng.8b04045
12. Lou Z, Han H, Zhou M, et al. (2018) Synthesis of magnetic wood with excellent and tunable electromagnetic wave-absorbing properties by a facile vacuum/pressure impregnation method. *ACS Sustainable Chem Eng* 6: 1000–1008. https://doi.org/10.1021/acssuschemeng.7b03332
13. Zhao S, Gao Z, Chen C, et al. (2016) Alternate nonmagnetic and magnetic multilayer nanofilms deposited on carbon nanocoils by atomic layer deposition to tune microwave absorption property. *Carbon* 98: 196–203. https://doi.org/10.1016/j.carbon.2015.10.101
14. Qiang R, Du Y, Wang Y, et al. (2016) Rational design of yolk-shell C@C microspheres for the effective enhancement in microwave absorption. *Carbon* 98: 599–606. https://doi.org/10.1016/j.carbon.2015.11.054
15. Xu H, Yin X, Zhu M, et al. (2017) Carbon hollow microspheres with a designable mesoporous shell for high-performance electromagnetic wave absorption. *ACS Appl Mater Interfaces* 9: 6332–6341. https://doi.org/10.1021/acsami.6b15826
16. Zhang N, Huang Y, Wang M (2018) 3D ferromagnetic graphene nanocomposites with ZnO nanorods and Fe_3O_4 nanoparticles co-decorated for efficient electromagnetic wave absorption. *Compos Part B-Eng* 136: 135–142. https://doi.org/10.1016/j.compositesb.2017.10.029

17. Zhang H, Xie A, Wang C, et al. (2013) Novel rGO/α-Fe_2O_3 composite hydrogel: Synthesis, characterization and high performance of electromagnetic wave absorption. *J Mater Chem A* 1: 8547–8552. https://doi.org/10.1039/c3ta11278k
18. Zhang N, Huang Y, Zong M, et al. (2017) Synthesis of ZnS quantum dots and $CoFe_2O_4$ nanoparticles co-loaded with graphene nanosheets as an efficient broad band EM wave absorber. *Chem Eng J* 308: 214–221. https://doi.org/10.1016/j.cej.2016.09.065
19. Trey S, Olsson RT, Ström V, et al. (2014) Controlled deposition of magnetic particles within the 3-D template of wood: Making use of the natural hierarchical structure of wood. *RSC Adv* 4: 35678–35685. https://doi.org/10.1039/c4ra04715j
20. Gan W, Gao L, Zhan X, et al. (2015) Hydrothermal synthesis of magnetic wood composites and improved wood properties by precipitation with $CoFe_2O_4$/hydroxyapatite. *RSC Adv* 5: 45919–45927. https://doi.org/10.1039/c5ra06138e
21. Lou Z, Zhang Y, Zhou M, et al. (2018) Synthesis of magnetic wood fiber board and corresponding multi-layer magnetic composite board, with electromagnetic wave absorbing properties. *Nanomaterials* 8: 1–14. https://doi.org/10.3390/nano8060441
22. Liu TT, Cao MQ, Fang YS, et al. (2022) Green building materials lit up by electromagnetic absorption function: A review. *J Mater Sci Technol* 112: 329–344. https://doi.org/10.1016/j.jmst.2021.10.022
23. Lou Z, Han X, Liu J, et al. (2021) Nano-Fe_3O_4/bamboo bundles/phenolic resin oriented recombination ternary composite with enhanced multiple functions. *Compos Part B-Eng* 226: 109335. https://doi.org/10.1016/J.COMPOSITESB.2021.109335
24. Oka H, Terui M, Osada H, et al. (2012) Electromagnetic wave absorption characteristics adjustment method of recycled powder-type magnetic wood for use as a building material. *IEEE Trans Magn* 48: 3498–3500. https://doi.org/10.1109/TMAG.2012.2196026
25. Pourjafar S, Rahimpour A, Jahanshahi M (2012) Synthesis and characterization of PVA/PES thin film composite nanofiltration membrane modified with TiO_2 nanoparticles for better performance and surface properties. *J Ind Eng Chem* 18: 1398–1405. https://doi.org/10.1016/j.jiec.2012.01.041
26. Oka H, Fujita H (1999) Experimental study on magnetic and heating characteristics of magnetic wood. *J Appl Phys* 85: 5732–5734. https://doi.org/10.1063/1.370267
27. Dong Y, Yan Y, Zhang S, et al. (2014) Wood/polymer nanocomposites prepared by impregnation with furfuryl alcohol and Nano-SiO2. *BioResources* 9: 6028–6040. https://doi.org/10.15376/biores.9.4.6028-6040
28. Rahayu I, Prihatini E, Ismail R, et al. (2022) Fast-growing magnetic wood synthesis by an in-situ method. *Polymers* 14: 2137. https://doi.org/10.3390/polym14112137
29. Zhang X, Zhou R, Rao W, et al. (2006) Influence of precipitator agents NaOH and NH_4OH on the preparation of Fe_3O_4 nano-particles synthesized by electron beam irradiation. *J Radioanal Nucl Chem* 270: 285–289. https://doi.org/10.1007/s10967-006-0346-8
30. Fajriani E, Ruelle J, Dlouha J, et al. (2013) Radial variation of wood properties of sengon (paraserianthes falcataria) and jabon (anthocephalus cadamba). *J Indian Acad Wood Sci* 10: 110–117. https://doi.org/10.1007/s13196-013-0101-z
31. Rahayu I, Darmawan W, Nugroho N, et al. (2014) Demarcation point between juvenile and mature wood in sengon (falcataria moluccana) and jabon (antocephalus cadamba). *J Trop For Sci* 26: 331–339. https://www.jstor.org/stable/43150914

32. Priadi T, Sholihah M, Karlinasari L (2019) Water absorption and dimensional stability of heat-treated fast-growing hardwoods. *J Korean Wood Sci Technol* 47: 567–578. https://doi.org/10.5658/WOOD.2019.47.5.567
33. Hadi YS, Massijaya MY, Abdillah IB, et al. (2020) Color change and resistance to subterranean termite attack of mangium (acacia mangium) and sengon (falcataria moluccana) smoked wood. *J Korean Wood Sci Technol* 48: 1–11. https://doi.org/10.5658/WOOD.2020.48.1.1
34. Hartati N, Sudarmonowati E, Fatriasari W, et al. (2010) Wood characteristic of superior sengon collection and prospect of wood properties improvement through genetic engineering. *Wood Res J* 1: 103–107. https://api.semanticscholar.org/CorpusID:89700771
35. Krisnawati H, Kallio M, Kanninen M (2011) *Anthocephalus Cadamba Miq.: Ecology, Silviculture and Productivity*, Bogor: Center for International Forestry Research. https://doi.org/10.17528/cifor/003481
36. Laksono GD, Rahayu IS, Karlinasari L, et al. (2023) Characteristics of magnetic sengon wood impregnated with nano Fe_3O_4 and furfuryl alcohol. *J Korean Wood Sci Technol* 51: 1–13. https://doi.org/10.5658/WOOD.2023.51.1.1
37. Jaunslavietis J, Shulga G, Ozolins J, et al. (2018) Hydrophilic-hydrophobic characteristics of wood-polymer composites filled with modified wood particle. *Key Eng Mater* 762: 176–181. https://doi.org/10.4028/www.scientific.net/KEM.762.176
38. Prihatini E, Wahyuningtyas I, Rahayu I, et al. (2022) Modification of fast-growing wood into magnetic wood with impregnation method using Fe_3O_4 nanoparticles. *J Sylva Lestari* 10: 211–222. https://doi.org/10.23960/jsl.v11i2.651
39. Tathod AP, Dhepe PL (2015) Efficient method for the conversion of agricultural waste into sugar alcohols over supported bimetallic catalysts. *Bioresource Technol* 178: 36–44. https://doi.org/10.1016/j.biortech.2014.10.036
40. Teng TJ, Arip MNM, Sudesh K, et al. (2018) Conventional technology and nanotechnology in wood preservation: A review. *BioResources* 13: 9220–9252. https://doi.org/10.15376/biores.13.4.Teng
41. Baysal E, Ozaki SK, Yalinkilic MK (2004) Dimensional stabilization of wood treated with furfuryl alcohol catalysed by borates. *Wood Sci Technol* 38: 405–415. https://doi.org/10.1007/s00226-004-0248-2
42. Dong Y, Yan Y, Zhang Y, et al. (2016) Combined treatment for conversion of fast-growing poplar wood to magnetic wood with high dimensional stability. *Wood Sci Technol* 50: 503–517. https://doi.org/10.1007/s00226-015-0789-6
43. Li F, Jiang S, Huang J, et al. (2019) Catalytic transfer hydrogenation of furfural to furfuryl alcohol over a magnetic Fe_3O_4@C catalyst. *New J Chem* 44: 478–486. https://doi.org/10.1039/c9nj04698d
44. Hou P, Ma M, Zhang P, et al. (2021) Catalytic transfer hydrogenation of furfural to furfuryl alcohol using easy-to-separate core–shell magnetic zirconium hydroxide. *New J Chem* 45: 2715–2722. https://doi.org/10.1039/d0nj05638c
45. Alibegovic K, Morgan G, Losovyj Y, et al. (2017) Efficient furfuryl alcohol synthesis from furfural over magnetically recoverable catalysts: Does the catalyst stabilizing medium matter? *ChemistrySelect* 2: 5485–5491. https://doi.org/10.1002/slct.201701100

46. Wahyuningtyas I, Rahayu IS, Maddu A, et al. (2022) Magnetic properties of wood treated with nano-magnetite and furfuryl alcohol impregnation. *BioResources* 17: 6496–6510. https://ojs.cnr.ncsu.edu/index.php/BRJ/article/view/22098
47. Cheng Z, Wei Y, Liu C, et al. (2020) Lightweight and construable magnetic wood for electromagnetic interference shielding. *Adv Eng Mater* 22: 1–24. https://doi.org/10.1002/adem.202000257
48. Zheng Y, Song Y, Gao T, et al. (2020) Lightweight and hydrophobic three-dimensional wood-derived anisotropic magnetic porous carbon for highly efficient electromagnetic interference shielding. *ACS Appl Mater Interfaces* 12: 40802–40814. https://doi.org/10.1021/acsami.0c11530
49. British Standard (1957) *Methods of Testing Small Clear Specimens of Timber*, London: British Standard Institution. Available from: https://allcivilstandard.com/wp-content/uploads/2019/02/BS-00373-1957-1999.pdf.
50. Peternele WS, Monge Fuentes V, Fascineli ML, et al. (2014) Experimental investigation of the coprecipitation method: An approach to obtain magnetite and maghemite nanoparticles with improved properties. *J Nanomater* 2014: 682985. https://doi.org/10.1155/2014/682985
51. Cornell RM, Schwertmann U (2003) *The Iron Oxides: Structure, Properties, Reactions, Occurencs and Uses*, Weinheim: Wiley. https://doi.org/10.1002/3527602097
52. Sompech S, Srion A, Nuntiya A (2012) The effect of ultrasonic treatment on the particle size and specific surface area of $LaCoO_3$. *Procedia Eng* 32: 1012–1018. https://doi.org/10.1016/j.proeng.2012.02.047
53. Oka H, Fujita H, Seki K (2000) Composition and heating efficiency of magnetic wood by induction heating. *IEEE Trans Magn* 36: 3715–3717. https://doi.org/10.1109/20.908950
54. Bowyer JL, Shmulsky R, Haygreen JG (2007) *Forest Products and Wood Science—An Introduction*, Iowa: Blackwell Publisher. https://doi.org/10.1002/9780470960035
55. Rowell RM, Ellis WD (1978) Determination of dimensional stabilization of wood using the water-soak method. *Wood Fiber Sci* 10: 104–111. https://wfs.swst.org/index.php/wfs/article/view/1004
56. Hill CAS (2006) *Wood Modification: Chemical, Thermal, and Other Processes*, West Sussex: Willey. https://doi.org/10.1002/0470021748
57. Gerasimov AM, Eremina OV, Cherkasova MV, et al. (2021) Application of particle-size analysis in various industries. *J Phys Conf Ser* 1728: 012003. https://doi.org/10.1088/1742-6596/1728/1/012003
58. Jayaprakash J, Srinivasan N, Chandrasekaran P (2014) Surface modifications of CuO nanoparticles using ethylene diamine tetra acetic acid as a capping agent by sol-gel routine. *Spectrochim Acta A* 123: 363–368. https://doi.org/10.1016/J.SAA.2013.12.080
59. Dubey V, Kain V (2018) Synthesis of magnetite by coprecipitation and sintering and its characterization. *Mater Manuf Process* 33: 835–839. https://doi.org/10.1080/10426914.2017.1401720
60. Fumis DB, Silveira MLDC, Gaglieri C, et al. (2022) The effect of EDTA functionalization on Fe_3O_4 thermal behavior. *Mat Res* 25: 1–6. https://doi.org/10.1590/1980-5373-MR-2022-0312
61. Magdalena AG, Silva IMB, Marques RFC, et al. (2018) EDTA-functionalized Fe_3O_4 nanoparticles. *J Phys Chem Solids* 113: 5–10. https://doi.org/10.1016/j.jpcs.2017.10.002

62. Wang M, Wang N, Tang H, et al. (2012) Surface modification of nano-Fe_3O_4 with EDTA and its use in H_2O_2 activation for removing organic pollutants. *Catal Sci Technol* 2: 187–194. https://doi.org/10.1039/c1cy00260k
63. Pereira SV, Colombo FB, De Freitas LAP (2016) Ultrasound influence on the solubility of solid dispersions prepared for a poorly soluble drug. *Ultrason Sonochem* 29: 461–469. https://doi.org/10.1016/j.ultsonch.2015.10.022
64. Dudchenko N, Pawar S, Perelshtein I, et al. (2022) Magnetite nanoparticles : Synthesis and applications in optics. *Materials* 15: 2601. https://doi.org/10.3390/ma15072601
65. Mascolo MC, Pei Y, Ring TA, et al. (2013) Room temperature co-precipitation synthesis of magnetite nanoparticles in a large pH window with different bases. *Materials* 6: 5549–5567. https://doi.org/10.3390/ma6125549
66. Khan I, Saeed K, Khan I (2019) Nanoparticles: Properties, applications and toxicities. *Arab J Chem* 12: 908–931. https://doi.org/10.1016/j.arabjc.2017.05.011
67. Fan S, Gao X, Pang J, et al. (2023) Enhanced preservative performance of pine wood through nano-xylan treatment assisted by high-temperature steam and vacuum impregnation. *Materials* 16: 3976. https://doi.org/10.3390/ma16113976
68. Yulianingsih R, Sugiarto Y, Putranto W (2015) Mass transfer characteristics during vacuum impregnation process of papaya fruit in sucrose solution. *JTP* 16: 159–166. https://jtp.ub.ac.id/index.php/jtp/article/view/515
69. Martawijaya A, Hadjodarsono S, Haji M (2005) *Atlas Kayu Indonesia*, 2 Eds., Bogor: IAWA Journal.
70. Praptoyo H (2005) Comparative study of two types sampling method for measuring cell proportion and fiber dimension on sengon salomon wood. *J Ilmu Teknologi Kayu Tropis* 3: 60–63.
71. Ishiguri F, Hiraiwa T, Iizuka K, et al. (2009) Radial variation of anatomical characteristics in paraserianthes falcataria planted in Indonesia. *IAWA J* 30: 343–352. https://doi.org/10.1163/22941932-90000223
72. Ibrahim NA, Salleh KM, Fudholi A, et al. (2022) Drying regimes on regenerated cellulose films characteristics and properties. *Membranes* 12: 445. https://doi.org/10.3390/membranes12050445
73. Ashjari M, Reza A (2010) Efficient dispersion of magnetite nanoparticles in the polyurethane matrix through solution mixing and investigation of the nanocomposite properties. *J Inorg Organomet Polym* 20: 213–219. https://doi.org/10.1007/s10904-010-9337-x
74. Saha MC, Kabir E, Jeelani S (2023) Enhancement in thermal and mechanical properties of polyurethane foam infused with nanoparticles. *Mater Sci Eng A* 479: 213–222. https://doi.org/10.1016/j.msea.2007.06.060
75. Garskaite E, Stoll SL, Forsberg F, et al. (2021) The accessibility of the cell wall in scots pine (Pinus sylvestris l.) sapwood to colloidal Fe_3O_4 nanoparticles. *ACS Omega* 6: 21719–21729. https://doi.org/10.1021/acsomega.1c03204
76. Li W, Ren D, Zhang X, et al. (2016) The furfurylation of wood: A nanomechanical study of modified wood cells. *BioResources* 11: 3614–3625. https://doi.org/10.15376/biores.11.2.3614-3625
77. Sharif HMA, Mahmood A, Cheng HY, et al. (2019) Fe_3O_4 nanoparticles coated with EDTA and Ag nanoparticles for the catalytic reduction of organic dyes from wastewater. *ACS Appl Nano Mater* 2: 5310–5319. https://doi.org/10.1021/acsanm.9b01250
78. Rahayu IS, Wahyuningtyas I, Zaini LH, et al. (2021) Physical properties of impregnated ganitri wood by furfuryl alcohol and nano-SiO_2. *IOP Conf Ser Earth Environ Sci* 891: 012012. https://doi.org/10.1088/1755-1315/891/1/012012

79. Hadi YS, Herliyana EN, Mulyosari D, et al. (2020) Termite resistance of furfuryl alcohol and imidacloprid treated fast-growing tropicalwood species as function of field test. *Appl Sci* 10: 6101. https://doi.org/10.3390/app10176101
80. Kong L, Guan H, Wang X (2018) In situ polymerization of furfuryl alcohol with ammonium dihydrogen phosphate in poplar wood for improved dimensional stability and flame retardancy. *ACS Sustainable Chem Eng* 6: 3349–3357. https://doi.org/10.1021/acssuschemeng.7b03518
81. Segmehl JS, Laromaine A, Keplinger T, et al. (2018) Magnetic wood by: In situ synthesis of iron oxide nanoparticles via a microwave-assisted route. *J Mater Chem C* 6: 3395–3402. https://doi.org/10.1039/c7tc05849g
82. Dirna FC, Rahayu I, Zaini LH, et al. (2020) Improvement of fast-growing wood species characteristics by MEG and nano SiO_2 impregnation. *J Korean Wood Sci Technol* 48: 41–49. https://doi.org/10.5658/WOOD.2020.48.1.41
83. Rahayu I, Darmawan W, Nawawi DS, et al. (2022) Physical properties of fast-growing wood-polymer nano composite synthesized through TiO_2 nanoparticle impregnation. *Polymers* 14: 4463. https://doi.org/10.3390/polym14204463
84. Ghani RSM, Lee MD (2021) Challenges of wood modification process for plantation eucalyptus: A review of Australian setting. *J Korean Wood Sci Technol* 49: 191–209. https://doi.org/10.5658/WOOD.2021.49.2.191
85. Thygesen LG, Barsberg S, Vena TM (2010) Studied by fluorescence spectroscopy and confocal laser. *Wood Sci Technol* 44: 51–65. https://doi.org/10.1007/s00226-009-0255-4
86. Scimeca M, Bischetti S, Lamsira HK, et al. (2018) Energy dispersive X-ray (EDX) microanalysis: A powerful tool in biomedical research and diagnosis. *Eur J Histochem* 62: 89–99. https://doi.org/10.4081/ejh.2018.2841
87. Waly SA, Shehata MM, Massoud A (2018) Destructive and nondestructive analysis of some modern coins using ICP-AES and PIXE techniques. *Chem Res J* 3: 1–8. Available from: https://chemrj.org/download/vol-3-iss-1-2018/chemrj-2018-03-01-01-08.pdf.
88. Bartz W, Górka M, Rybak J, et al. (2021) The assessment of effectiveness of SEM- EDX and ICP-MS methods in the process of determining the mineralogical and geochemical composition of particulate matter deposited on spider webs. *Chemosphere* 278: 130454. https://doi.org/10.1016/j.chemosphere.2021.130454
89. He M, Xu D, Li C, et al. (2020) Cell wall bulking by maleic anhydride for wood durability improvement. *Forests* 11: 367. https://doi.org/10.3390/F11040367
90. Gaitán-Alvarez J, Berrocal A, Lykidis C, et al. (2021) Furfurylation of tropical wood species with and without silver nanoparticles: Part II: Evaluation of wood properties. *Wood Mater Sci Eng* 18: 1112–119. https://doi.org/10.1080/17480272.2021.1992795
91. Sundrarajan M, Ramalakshmi M (2012) Novel cubic magnetite nanoparticle synthesis using room temperature ionic liquid. *E-J Chem* 9: 541254. https://doi.org/10.1155/2012/541254
92. Xu YH, Huang C (2011) Effect of sodium periodate selective oxidation on crystallinity of cotton cellulose. *Adv Mat Res* 197–198: 1201–1204. https://doi.org/10.4028/www.scientific.net/AMR.197-198.1201
93. Wang C, Piao C, Lucas C (2010) Synthesis and characterization of superhydrophobic wood surfaces. *J Appl Polym Sci* 116: 2658–2667. https://doi.org/10.1002/app.32844

94. Gan W, Gao L, Liu Y, et al. (2016) The magnetic, mechanical, thermal properties and UV resistance of $CoFe_2O_4/SiO_2$-coated film on wood. *J Wood Chem Technol* 36: 94–104. https://doi.org/10.1080/02773813.2015.1074247
95. Coates J (2006) Interpretation of infrared spectra, a practical approach, In: Meyers RA, McKelvy ML, *Encyclopedia of Analytical Chemistry*, Weinheim: Wiley. https://doi.org/10.1002/9780470027318.a5606
96. Kim T, Assary RS, Kim H, et al. (2013) Effects of solvent on the furfuryl alcohol polymerization reaction: UV Raman spectroscopy study. *Catal Today* 205: 60–66. https://doi.org/10.1016/j.cattod.2012.09.033
97. Pranger LA, Nunnery GA, Tannenbaum R (2012) Mechanism of the nanoparticle-catalyzed polymerization of furfuryl alcohol and the thermal and mechanical properties of the resulting nanocomposites. *Compos Part B-Eng* 43: 1139–1146. https://doi.org/10.1016/j.compositesb.2011.08.010
98. Lin CC, Ho JM (2014) Structural analysis and catalytic activity of Fe_3O_4 nanoparticles prepared by a facile co-precipitation method in a rotating packed bed. *Ceram Int* 40: 10275–10282. https://doi.org/10.1016/j.ceramint.2014.02.119
99. Lou Z, Wang Q, Sun W, et al. (2022) Regulating lignin content to obtain excellent bamboo-derived electromagnetic wave absorber with thermal stability. *Chem Eng J* 430: 133178. https://doi.org/10.1016/j.cej.2021.133178
100. Wan Nor WFK, Soh SKC, Azmi AAAR, et al. (2018) Synthesis and physicochemical properties of magnetite nanoparticles (Fe_3O_4) as potential solid support for homogeneous catalysts. *Malaysian J Anal Sci* 22: 768–774. https://doi.org/10.17576/mjas-2018-2205-04
101. Gieroba B, Krysa M, Wojtowicz K, et al. The FT-IR and raman spectroscopies as tools for biofilm characterization created by cariogenic streptococci. *Int J Mol Sci* 21: 3811. https://doi.org/10.3390/ijms21113811
102. Wang LL, Li N, Zhao T, et al. (2019) Magnetic properties of $FeNi_3$ nanoparticle modified pinus radiata wood nanocomposites. *Polymers* 11: 421. https://doi.org/10.3390/polym11030421
103. Ramadani IWS (2015) *Characterization of Line Broadening and $2\theta_0$ Correction in X-Ray Diffraction Analysis,* Surabaya: Sepuluh Nopember Institute of Technology. Available from: https://repository.its.ac.id/71784/1/1113201044-Master%20Thesis.pdf.
104. Agarwal UP, Reiner RR, Ralph SA (2011) Cellulose crystallinity of woods, wood pulps, and agricultural fibers by FT-Raman spectroscopy. 16th International Symposium on Wood, Fiber, and Pulping, 1: 69–74.
105. Fadli A, Komalasari, Adnan A, et al. (2019) Synthesis of magnetite nanoparticles via co-precipitation method. *IOP Conf Ser Mater Sci Eng* 622: 1–7. https://doi.org/10.1088/1757-899X/622/1/012013
106. Batista NL, Olivier P, Bernhart G, et al. (2016) Correlation between degree of crystallinity, morphology and mechanical properties of PPS/carbon fiber laminates. *Mat Res* 19: 195–201. https://doi.org/10.1590/1980-5373-MR-2015-0453
107. Sejati PS, Akong FO, Torloting C, et al. (2022) Fully wood based novel translucent and thermoplastic materials by solvent-free esterification. *RSC Adv* 12: 35206–35214. https://doi.org/10.1039/d2ra06555j

108. Susanti S (2014) *Crystal Structure Study Magnetic Nanoparticles (Fe_3O_4) as a Function of Temperature Synthesis of Results Using Sonochemical*. Yogyakarta: Universitas Islam Negeri Sunan Kalijag.
109. Ström V, Olsson RT, Rao KV. (2010) Real-time monitoring of the evolution of magnetism during precipitation of superparamagnetic nanoparticles for bioscience applications. *J Mater Chem* 20: 4168–4175. https://doi.org/10.1039/c0jm00043d
110. Fadia SL, Rahayu I, Nawawi DS, et al. (2023) The physical and magnetic properties of sengon (falcataria moluccana) wood impregnated with synthesized magnetite nanoparticles. *J Sylva Lestari* 11: 408–426. https://doi.org/10.23960/jsl.v11i3.761
111. Li Z, Chanéac C, Berger G, et al. (2019) Mechanism and kinetics of magnetite oxidation under hydrothermal conditions. *RSC Adv* 9: 33633–33642. https://doi.org/10.1039/c9ra03234g
112. Yu BY, Kwak SY (2010) Assembly of magnetite nanoparticles into spherical mesoporous aggregates with a 3-D wormhole-like porous structure. *J Mater Chem* 20: 8320–8328. https://doi.org/10.1039/C0JM01274B
113. Prihatini E, Ismail R, Rahayu IS, et al. (2023) Uji performa alat vakum tekan termodifikasi untuk impregnasi kayu. *J Pengelolaan Lab Pendidik* 5: 75–82. https://doi.org/10.14710/jplp.5.2.75-82
114. Tebriani S, Rifai H (2016) Analisis pengaruh ukuran bulir serta domain magnetik terhadap kesuburan tanah perkebunan sawit. *Nat Sci J* 4: 616–627. https://ejournal.uinib.ac.id/jurnal/index.php/naturalscience/article/view/454
115. Tang T, Fu Y (2020) Formation of chitosan/sodium phytate/nano-Fe_3O_4 magnetic coatings on wood surfaces via layer-by-layer self-assembly. *Coatings* 10: 51. https://doi.org/10.3390/coatings10010051
116. Umehara Y, Endo H, Watanabe M, et al. (2018) Frequency spectra of vibration transmissibility for magnetic elastomers with various plasticizer contents. *AIMS Mater Sci* 5: 44–53. https://doi.org/10.3934/matersci.2018.1.44
117. Lam UT, Mammucari R, Suzuki K, et al. (2008) Processing of iron oxide nanoparticles by supercritical fluids. *Ind Eng Chem Res* 47: 599–614. https://doi.org/10.1021/ie070494+
118. Inoue A, Kong F (2022) Soft magnetic materials, In: Olabi AG, *Encyclopedia of Smart Materials*, Oxford: Elsevier, 10–23. https://doi.org/10.1016/B978-0-12-803581-8.11725-4
119. Moya R, Gait J, Berrocal A, et al. (2022) In situ synthesis of Fe_3O_4 nanoparticles and wood composite properties of three tropical species. *Materials* 15: 3394. https://doi.org/10.3390/ma15093394
120. Saxena N, Singh M (2017) Efficient synthesis of superparamagnetic magnetite nanoparticles under air for biomedical applications. *J Magn Magn Mater* 429: 166–176. https://doi.org/10.1016/j.jmmm.2017.01.031
121. Fliegans J, Rado C, Soulas R, et al. (2021) Revisiting the demagnetization curves of Dy-diffused Nd-Fe-B sintered magnets. *J Magn Magn Mater* 520: 1–29. https://doi.org/10.1016/j.jmmm.2020.167280
122. Nypelö T (2022) Magnetic cellulose: Does extending cellulose versatility with magnetic functionality facilitate its use in devices? *J Mater Chem C* 10: 805–818. https://doi.org/10.1039/d1tc02105b
123. Kirupakar BR, Vishwanath BA, Padma SM, et al. (2016) Vibrating sample magnetometer and its application in characterisation of magnetic property of the anti cancer drug magnetic microspheres. *Int J Pharm Drug Anal* 4: 227–233.

124. Schoppa A, Delarbre P (2014) Soft magnetic powder composites and potential applications in modern electric machines and devices. *IEEE Trans Magn* 50: 4–7. https://doi.org/10.1109/TMAG.2013.2290135
125. Ying Y, Hu L, Li Z, et al. (2023) Preparation of densified fine-grain high-frequency MnZn ferrite using the cold sintering process. *Materials* 16: 3454. https://doi.org/10.3390/ma16093454
126. Wang S, Zheng J, Zheng D, et al. (2022) Low core losses of Fe-based soft magnetic composites with an Zn-O-Si insulating layer obtained by coupling synergistic photodecomposition. *Materials* 15: 8660. https://doi.org/10.3390/ma15238660
127. Das R, Ye L, Lal SS, et al. (2023) Fabrication and soft magnetic properties of FeSiB based flakes with insulating surface layer suitable for high frequency power applications. *AIP Adv* 13: 025210. https://doi.org/10.1063/9.0000406
128. Nguyen KDV, Vo KDN (2020) Magnetite nanoparticles-TiO_2 nanoparticles-graphene oxide nanocomposite: Synthesis, characterization and photocatalytic degradation for Rhodamine-B dye. *AIMS Mater Sci* 7: 288–301. https://doi.org/10.3934/MATERSCI.2020.3.288

AIMS Press